A peer-reviewed version of this preprint was published in PeerJ on 20 December 2016.

View the peer-reviewed version (peerj.com/articles/2805), which is the preferred citable publication unless you specifically need to cite this preprint.

Silva PJ. 2016. Refining the reaction mechanism of O_2 towards its co-substrate in cofactor-free dioxygenases. PeerJ 4:e2805
https://doi.org/10.7717/peerj.2805

Refining the reaction mechanism of O_2 towards its substrate in cofactor-free dioxygenases

Pedro J Silva Corresp. [1]

[1] FP-ENAS/Fac. de Ciências da Saúde, Universidade Fernando Pessoa, Porto, Portugal

Corresponding Author: Pedro J Silva
Email address: pedros@ufp.edu.pt

Cofactor-less oxygenases perform challenging catalytic reactions between singlet substrates and triplet oxygen, in spite of apparently violating the spin-conservation rule. In bacterial ring-cleaving 2,4-dioxygenase, the active site has been suggested by quantum chemical computations to fine tune triplet oxygen reactivity, allowing it to interact rapidly with its singlet substrate without the need for spin inversion, and in urate oxidase the reaction is thought to proceed through electron transfer from the deprotonated substrate to an aminoacid sidechain, which then feeds the electron to the oxygen molecule. In this work, we perform additional quantum chemical computations on these two systems to elucidate several intriguing features unaddressed by previous workers. These computations establish that in both enzymes the reaction proceeds through direct electron transfer from substrate to O_2 followed by radical recombination, instead of minimum-energy crossing points between singlet and triplet potential energy surfaces without formal electron transfer. The active site does not affect the reactivity of oxygen directly but is crucial for the generation of the deprotonated form of the substrates, which have redox potentials far below those of their protonated forms and therefore may transfer electrons to oxygen without sizeable thermodynamic barriers. This mechanism seems to be shared by most cofactor-less oxidases studied so far.

Introduction

Reactions where the number of unpaired electrons changes as reactants are transformed into products are not generally allowed by quantum mechanics due to Wigner's spin-conservation rule. This rule prevents the dioxygen molecule, which has two unpaired electrons and a S=1 (triplet) ground state, from easily reacting with acceptors in the singlet state (S=0, like most organic molecules) to yield organic products without unpaired electrons. Such reactions are not, however, strictly impossible due to the intervention of spin-orbit coupling, which mixes both spin states. Understanding spin-forbidden reactions requires the characterization of the potential energy surfaces of the different spin-states involved in the reaction, and the location of the point where both surfaces touch each other(Harvey, 2007, 2014). At this specific geometry (the "minimum-energy crossing point", henceforth abbreviated as MECP) the system may transition (or "hop") between spin systems, with a probability which depends on the magnitude of the spin-orbit coupling and may be computed approximately according to the Landau-Zener equation(Nakamura, 1987). Since spin-orbit coupling is a relativistic effect which increases with the nuclear charge, formally spin-forbidden reactions become progressively easier as one descends down the periodic table, to the point that "spin-forbidden" transitions involving Ni, Cu or elements of the 5th (or lower) periods are as probable as "spin-allowed" transitions (Marian, 2001). Proteins which generate, use or transport dioxygen therefore usually rely on transition metals such as manganese, copper and iron(Ferguson-Miller & Babcock, 1996; Que & Ho, 1996; Sono et al., 1996; Wallar & Lipscomb, 1996; Yachandra, Sauer & Klein, 1996). A large class of enzymes devoid of metals (the flavoproteins) circumvents the problem with the help of flavin, which readily transfers one electron to oxygen yielding a separated radical pair consisting of a

superoxide anion and a flavin-based radical (Massey, 1994). This separated radical-pair readily recombines after a "flip" of the spin in the superoxide anion, yielding a peroxide product with no unpaired electrons.

Several enzymes catalyze the addition of oxygen to suitably (π-conjugated) substrates in spite of lacking flavin or metals in their active sites, often through "substrate-assisted catalysis" (Fetzner & Steiner, 2010) which takes advantage of the enhanced reactivity of these conjugated system upon enzyme-promoted substrate deprotonation. Extensive computational details of the reaction mechanisms of coproporphyrinogen oxidase (Silva & Ramos, 2008) and vitamin K.-dependent glutamate carboxylase (Silva & Ramos, 2007) confirmed that substrate deprotonation is indeed required for their catalytic action. Evidence for substrate deprotonation is also available for urate oxidase (Bui et al., 2014), although in this instance a more complex mechanism involving transient protein-based free radicals was proposed to be operative, based on EPR measurements of anaerobic preparations of substrate-bound enzyme (Gabison et al., 2011). Based on the reaction profile towards a superoxide-scavenging spin probe, flavin-like reactivity towards O_2 has also been suggested to occur (Thierbach et al., 2014) in a bacterial ring-cleaving 2,4-dioxygenase active towards (1*H*)-3-hydroxy-4-oxoquinolines (EC 1.13.11.47), but recent computational results (Hernández-Ortega et al., 2015) have been interpreted as contradicting this hypothesis, as the computed reaction energy for the electron transfer from substrate to O_2 (8-11 kcal·mol^{-1}) would imply an "endothermic process […] unlikely to happen spontaneously in the protein or in solvent" (Hernández-Ortega et al., 2015). As an alternative, these workers computed the energetics of a pathway (Figure 1) consisting of addition of triplet oxygen to the deprotonated substrate (yielding a triplet peroxide, $^3I_1$, 17 kcal·mol^{-1} above the reactants), followed by a transition to a singlet peroxide state ($^1I_1$, 8 kcal·mol^{-1} below the triplet state, i.e. 9

kcal·mol^{-1} above the reactant state). Minimum-energy crossing points between the singlet and triplet potential energy surfaces were not located in that work, but were predicted to lie around 10 kcal·mol^{-1} above the reactant state.

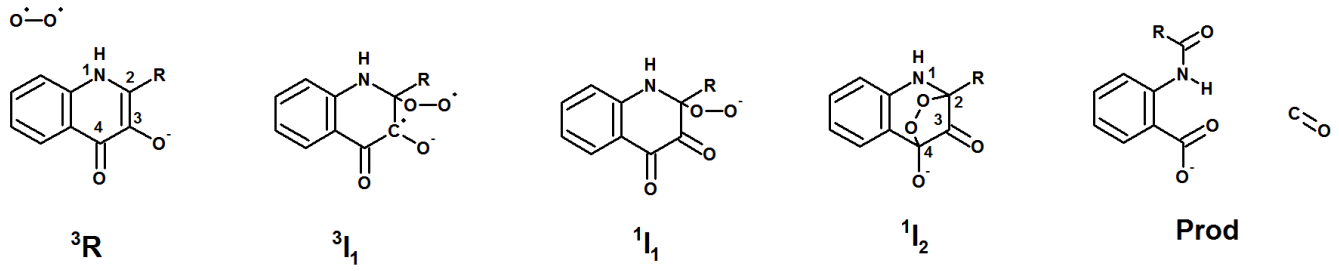

Some of the conclusions of the computational work of Hernandéz-Ortega *et al.* seem problematic: on the one hand, the computed 8-11 kcal·mol^{-1} endothermicity of the electron-transfer process from substrate to triplet oxygen does not seem enough to discard the possibility of an electron-transfer mechanism, since larger activation free energies of 17.4 kcal·mol^{-1} are able, according to transition state theory, of sustaining reaction rates of 1s^{-1} at room temperature; and on the other hand, the lack of data on the relative energies of the excited singlet state of the triplet peroxide intermediate and of the triplet state of the singlet peroxide intermediate leave open the possibility that those two potential energy surfaces do not cross between ^{3}I$_1$ and ^{1}I$_1$, and that the minimum-energy crossing point actually lies between the reactant state (^{3}R) and the singlet intermediate ^{1}I$_1$, thereby completely bypassing the putative triplet peroxide (^{3}I$_1$). In this work we perform additional computational studies of the putative intermediates of this reaction and conclude that the triplet peroxide state is never formed: the reaction instead proceeds directly from ^{3}R to ^{1}I$_1$ either through low-lying minimum-energy crossing points or, most likely, through direct electron-transfer from substrate to oxygen in flavin-like fashion. Additional computations in model systems for other reactions catalyzed by cofactor-less oxygenases strongly suggest that such flavin-like reactivity should be the norm for inductively activated π-conjugated substrates.

Computational methods

Quantum chemical computations were performed with the Firefly(Granovsky, 2013) quantum chemistry package, which is partially based on the GAMESS (US)(Schmidt et al., 1993) source code. As in the original work (Hernández-Ortega et al., 2015), all computations were performed with the B3LYP density-functional (Lee, Yang & Parr, 1988; Becke, 1993; Hertwig & Koch, 1995). Optimized geometries of large models of intermediates ^{3}R, $^{3}I_1$ and $^{1}I_1$ were obtained from the Supporting information of (Hernández-Ortega et al., 2015). Solution energies (Tomasi & Persico, 1994; Mennucci & Tomasi, 1997; Cossi et al., 1998) in water (ε=78.34) and chlorobenzene (ε=5.7, mimicking the less polar environment of the protein active site) of the singlet and triplet states of these molecules were computed using the 6-31G(d,p) basis set complemented with diffuse functions on the oxygen atoms to allow a better description of the oxygen-based anionic species (henceforth referred to as basis set BS1) .

Due to computational limitations, the search of minimum energy crossing points (MECP) between non-interacting singlet and triplet states required extensive trimming of the reaction model, which was reduced to the substrate, a water molecule, and the sidechains of the active-site dyad His_{251}/Asp_{126} responsible for substrate deprotonation. MECP were located employing the methodology developed by (Harvey et al., 1998) at the B3LYP/BS1 level. Since MECP optimization in gas phase yield very different geometries from continuum MECP optimizations(Silva & Ramos, 2007), we performed this search with a PCM continuum model using water as the solvent. The C_β atoms of His251 and Asp126 were kept frozen to limit system flexibility to that possible in the enzyme active site. Investigation of CO release step were performed with the larger model suggested by Aitor-Hernández et al. (including the sidechains of

His38, His100, Ser101, His102, Asp126, Trp160, His251, and the backbone amide linking Trp36 to Cys37), with several atoms kept fixed to prevent unrealistic movements. The fixed atoms were: C_β of His100 and His102, C_α of Ser101, Trp36 and Cys37, C_β and C_γ of His38, His251 and Trp160 and C_α and C_β of Asp126. Very fine two-dimensional scans of the potential energy surface at the B3LYP/6-31G(d) level were performed by simultaneously varying the C_3-C_4 and the O-O distances (while keeping the C_2-C_3 distance fixed to prevent hysteresis). While the size of the system prevented the numerical computation (and updating) of the hessians needed for saddpe point optimization, this scanning procedure procedure allowed the generation of smooth potential energy surfaces which enabled the location of high quality transition structure guesses.

The activation energy of the one-electron transfer between substrates and O_2 were estimated by applying Marcus theory for electron transfer, as suggested by Blomberg & Siegbahn (2003) and subsequently modified by Silva and Ramos (Silva & Ramos, 2008). As in previous works by our and other groups (Silva & Ramos, 2008, 2009; Silva, 2014; Wijaya et al., 2016) reorganization energies for every molecule in both oxidation states were computed using the water-optimized reactant geometries for the product state (and vice-versa) and activation energies were then computed by building appropriate Marcus parabolas using these reorganization energies. The smaller size of these models allowed us to increase the size of the basis set in these computations to 6-311G(d,p), while keeping the diffuse functions on the oxygen atoms to allow a better description of the oxygen-based anionic species (henceforth this basis set will be referred to as BS2). Atomic charge and spin density distributions were calculated with a Mulliken population analysis(Mulliken, 1955) based on symmetrically orthogonalized orbitals(Löwdin, 1970).

Computation of the binding modes of 2-methyl- and 2-butyl-(1*H*)-3-hydroxy-4-oxoquinoline towards 2,4-dioxygenase (PDB:2WJ4(Steiner et al., 2010)) were performed in YASARA

Structure (Krieger & Vriend, 2014) using its AutoDock VINA module with default parameters (Trott & Olson, 2010). The docking region was confined to a 39.8×34.8×34.8 Å box centered on residues Trp36, His38, His100, Ser101, His102, Asp126, Trp160, and His251. Residues Gly35, Trp36, His38, His100, Ser101, His102, Leu128, Phe136, Leu156, Trp160, Met177,Trp185, Ile192 and His251 were kept flexible during the docking procedure.

Results

*Bacterial ring-cleaving 2,4-dioxygenase active towards (1*H*)-3-hydroxy-4-oxoquinolines*

We started the search for minimum-energy crossing points between the triplet and singlet states of O_2 and deprotonated (1*H*)-3-hydroxy-4-oxoquinolines from the reported structures of the $^3I_1$ intermediate. To keep the computations tractable most of the surrounding aminoacids were excised, and only the Asp-His dyad responsible for the initial deprotonation of substrate (Steiner et al., 2010; Hernandez-Ortega et al., 2014) and charge stabilization of the $^3I_1/^1I_1$ intermediates was kept. Table 1 shows that this truncation has very modest effects on the reaction energetics, and should therefore not introduce relevant errors.

Table 1: Comparison of the quality of the energies obtained with the truncated model which includes only the substrate and the Asp/His dyad vs. the energies obtained with the large model used by (Hernández-Ortega et al., 2015). All energies are computed vs. the respective reactant state at the B3LYP/BS1 theory level in water. The large model includes the sidechains of His38, His100, Ser101, His102, Asp126, Trp160, His251, and the backbone amide linking Trp36 to Cys37. All coordinates were taken from the Supporting information of (Hernández-Ortega et al., 2015) and used without further optimization.

Quinoline substituent	Model used	$^3I_1$	$^1I_1$
-F	Large model	5.5	-10.1
-F	His_{251}/Asp_{126} + substrate	5.3	-10.1
- CH_3	Large model	12.6	0.6
- CH_3	His_{251}/Asp_{126} + substrate	13.5	1.2
-$(CH_2)_4CH_3$	Large model	19.2	4.8
-$(CH_2)_4CH_3$	His_{251}/Asp_{126} + substrate	18.7	1.5
-NO2	Large model	19.0	7.2
-NO2	His_{251}/Asp_{126} + substrate	24.0	10.6

As in the work we criticize (Hernandez-Ortega et al., 2014), all computations were repeated for four different (1*H*)-3-hydroxy-4-oxoquinolines to ascertain the influence of different substituents (methyl, pentyl, fluor and nitro) in the reaction course. The minimum-energy crossing points found (Figure 2) were dramatically different from the $^3I_1$ intermediates postulated in the previous work, which contain extremely short (1.499-1.502 Å) substrate-oxygen bonds and longer O-O bonds (1.38 Å) than observed for free superoxide (1.334 Å). The sole exception was found to be the fluoro-substituted substrate, which presented a short (1.56 Å) C-O distance (Table 2) and where the spin distribution at the triplet state (Figure 2) was the most different from the initial reactant state. In spite of the large change relative to the initial state, the MECP for this substrate proved to be the most energetically accessible of all the tested quinolines. Geometry optimizations of the triplet state starting from these MECP geometries invariably yielded the triplet reactant state and optimizations of the singlet state starting from this same geometry invariably collapsed into $^1I_1$ intermediates. This entails that the reaction will most likely proceed directly through the MECP and thence to $^1I_1$ and that the $^3I_1$ intermediates, in spite of lower energies than the minimum-energy crossing points (Table 2), are unproductive.

Table 2: Characterization of the minimum-energy crossing points between the singlet and triplet surfaces of oxygen:(1*H*)-3-hydroxy-4-oxoquinoline systems in the presence of the His_{251}/Asp_{126} catalytic dyad, at the B3LYP/BS1 level in a water continuum. The C_β atoms of His251 and Asp126 were kept frozen to limit system flexibility to that possible in the enzyme active site. [a:] Large model, including the sidechains of His38, His100,Ser101,His102, Asp126, Trp160, His251, and the backbone of Trp36, at B3LYP/BS1 in a water continuum. For the large

161 model coordinates were taken from the Supporting information of (Hernández-Ortega et al.,
162 2015) and used without further reoptimization.

163

Quinoline substituent:	$-(CH_2)_4CH_3$	$-CH_3$	-F	$-NO_2$
C-O distance (Å) at the MECP	2.308	2.23	1.568	1.968
O-O distance (Å) at the MECP	1.303	1.307	1.326	1.304
MECP Energy (kcal·mol^{-1}) vs. reactants	16.8	15.2	9.2	24.2
$^1I_1$ Energy (kcal·mol^{-1}) vs. reactants	11.1	9.0	-3.4	15.6
$^3I_1$ Energy (kcal·mol^{-1}) vs. reactants[a]	19.2	12.6	5.5	19.0

164

165

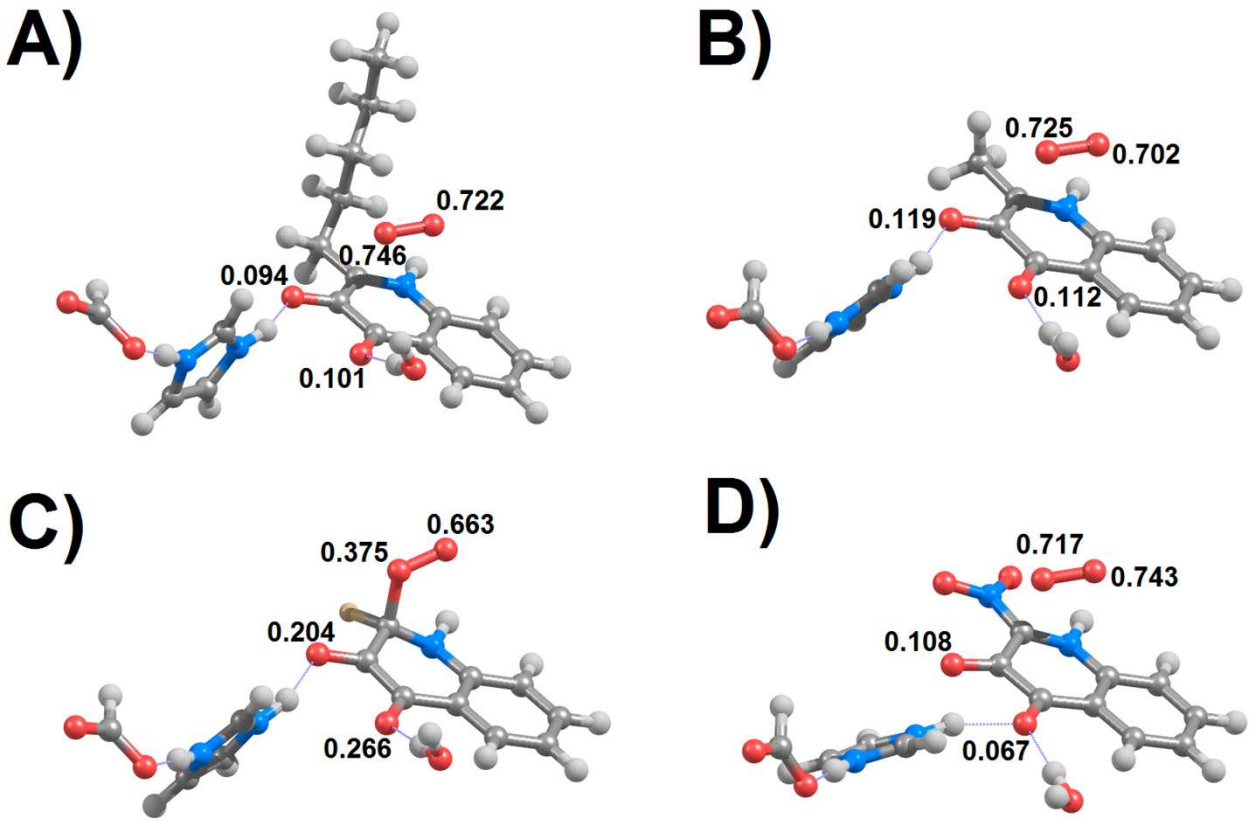

166

167

168 Figure 2: Optimized B3LYP/BS1 geometries of the minimum-energy crossing points of (1*H*)-
169 3-hydroxy-4-oxoquinolines bearing pentyl (A),methyl (B), fluoro (C) and nitro (D) substituents.
170 Spins on the oxygen atoms are shown for the triplet state at each of these geometries.

171

172 A preference for direct electron transfer to O_2 instead of a pathway relying on minimum-
173 energy crossing points between surfaces of different spin multiplicity has been postulated before
174 (e.g. (Massey, 1994)) for the flavin:O_2 system and confirmed by quantum chemical computations
175 (Prabhakar et al., 2002). Such preference is not limited to flavins, and has also been confirmed
176 computationally for the deprotonated pyrrole in the reaction catalyzed by the oxygen-dependent
177 coproporphyrinogen oxidase(Silva & Ramos, 2008). We have therefore analyzed the

178 thermodynamic and kinetic feasibility of direct electron transfer from substituted quinolines to
179 O_2 (Table 3). The reaction rate was found to be strongly correlated with the electron-donating
180 capability of the quinoline substituent (Table 3). For electron-donating and weakly-withdrawing
181 substituents the reaction rate can be extremely fast, regardless of the polarity of the solvent. Polar
182 environments generally lower the activation energy of this electron-transfer, enabling it to occur
183 at rates exceeding 0.1 s^{-1} even for such electron-withdrawing substituents as acetyl, nitro or
184 nitrile. Comparison of these activation energies to the energies of the minimum-energy crossing
185 points (Table 2) shows that the direct electron transfer route is favored for all tested substituents,
186 especially at higher dielectric constants. The generation of the peroxide intermediate $^1I_1$ is
187 therefore most likely to proceed (in agreement with the proposal by (Thierbach et al., 2014) and
188 in contrast to the mechanism postulated by (Hernández-Ortega et al., 2015)) through electron
189 transfer from substrate to O_2, followed by recombination of the substrate-based radical with
190 superoxide.
191
192 Table 3: Reaction energies and activation energies of the electron-transfer from substituted
193 (1*H*)-3-hydroxy-4-oxoquinolines to dioxygen, at the B3LYP/BS2//B3LYP/BS1 level. Unless
194 otherwise noted, the 3-hydroxyl group remained in the deprotonated state. Substituents are shows
195 ordered by increased values of their Hammet σ_m parameters (Hansch, Leo & Taft, 1991).
196

	In chlorobenzene		In water	
Quinoline substituent	Activation Energy ($kcal \cdot mol^{-1}$)	Reaction Energy ($kcal \cdot mol^{-1}$)	Activation Energy ($kcal \cdot mol^{-1}$)	Reaction energy ($kcal \cdot mol^{-1}$)

$-NH_2$	3.4	-1.5	2.0	-4.8
$-COO^-$	1.5	-5.1	5.9	4.4
$-(CH_2)_4CH_3$	7.1	6.0	5.2	3.0
$-CH_3$	6.8	5.5	4.9	2.5
$-CH_3$ (protonated quinoline)	86.2	58.1	46.9	38.7
-F	11.1	10.9	8.6	7.8
$-COCH_3$	22.5	21.5	16.6	16.5
-CN	24.6	22.9	18.3	18.0
-NO	23.9	23.7	20.0	20.0
$-NO_2$	41.2	33.1	31.1	27.5

Hernández-Ortega *et al.* have shown that the peroxide intermediate $^1I_1$ quickly becomes an endoperoxide ($^1I_2$) through attack of the substrate C_4 by the terminal oxygen. Release of C=O from $^1I_2$ yields a carboxylate function on C_4 and occurs quickly due to the stabilization of the nascent negative charge by hydrogen bonding with Ser101 (1.51 Å) and strong interaction with the positively-charged His251 (2.16 Å). In their computational investigation of this reaction step with quinolines bearing the much longer pentyl substituent, these researchers observed a remarkable increase of the activation energy for CO release of almost 20 kcal·mol^{-1}. Inspection of the structure of the transition state of the transformation of $^1I_2$ into products reveals that the high activation energy of the pentyl-substituted quinoline is due to the use of the same binding mode for this quinoline as for the methyl-substituted quinoline, which introduces steric clashes between the pentyl-group and His38, His100 and the Trp36-Cys37 backbone. To avoid these clashes, the pentyl-substituted substrate is forced to rotate 30º around the axis perpendicular to the quinoline ring, thus increasing the separation between the substrate and Ser101 (to 1.85 Å)

211 and His251 (to 2.67 Å), and strongly decreasing the charge stabilization provided by these
212 residues on the nascent carboxylate (Figure 3).

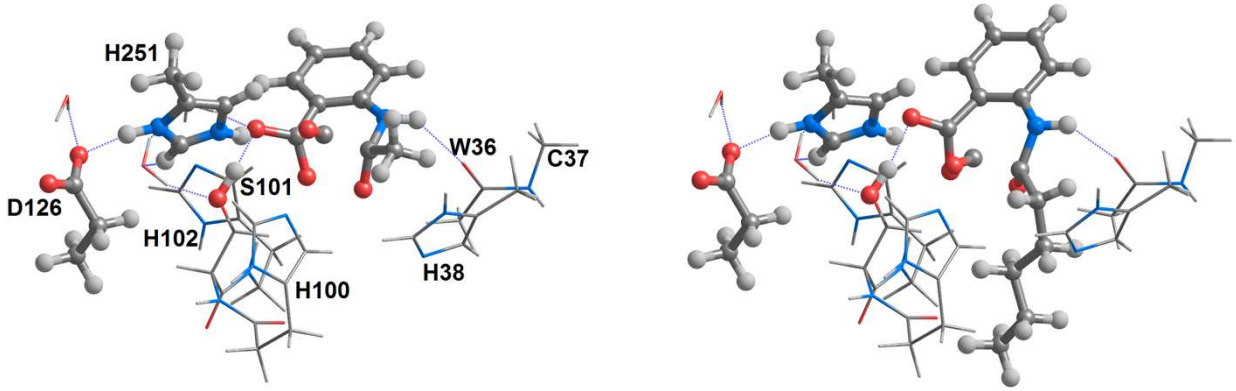

Figure 3: Proposed geometries of the transition states for the $^1I_2$→product reaction step for the A) methyl-, and B) pentyl-substituted 4-oxoquinolines. Coordinates taken from the Supporting information of (Hernández-Ortega et al., 2015). Trp160 has been omitted from images for clarity.

Although the 20 kcal·mol^{-1} increase of activation energy for the CO release step in the pentyl-substituted was regarded by the original researchers (Hernández-Ortega et al., 2015) as "in agreement with the drop in [experimental] rate constant" reported earlier in the same paper for the butyl-substituted substrate, the observed 30% increase in k_{cat} and 10-fold decrease of k_{cat}/K_M are not consistent with the 14-15 orders of magnitude difference in k_{cat} expected from such a difference in activation energy. Additional evidence against the mechanistic relevance of the proposed binding mode for the pentyl-substituted substrate comes from the superposition of the transition state model coordinates with the crystallographic structure of the enzyme: even after this 30º rotation, the proposed position of pentyl group lies on the space occupied by the Pro35-Gly36 stretch of the enzyme, which had been left out of the active site model. Long hydrocarbon substituents may, however, be accommodated if a binding mode rotated by 240º is assumed,

232 which places the aliphatic chain in the entrance channel bordered by Leu128, Phe136, Leu165,
233 Val159, Trp160, Gln221 and His251. This binding mode was confirmed as the best hit in
234 docking computations using Autodock VINA. A subsequent two-dimensional scan of the
235 coordinates involved in the $^1I_2$→product transition showed that in this binding mode a very low
236 energy pathway for CO release is accessible through a transition structure stabilized through
237 interactions with Ser101 and His251 (Figure 4B and Table 4). An identical scan was performed
238 for the methyl-substituted quinolone in the original orientation (Table 4 Figure 4, panels C and
239 D). The small differences in activation energies between both 4-oxoquinolines are fully
240 consistent with the lack of dramatic differences in the experimentally-measured kinetic
241 parameters.
242
243 Table 4: Comparison of the transition states of the CO release step for methyl- and butyl-
244 substituted quinolones. a: structure obtained from very fine 2D-scans, with an active site model
245 including the sidechains of His38, His100,Ser101,His102, Asp126, Trp160, His251, and the
246 backbone of Trp36. b: structure obtained from a complete saddle-point optimization in a minimal
247 model including only the substrate, a water molecule and a methanol molecule mimicking
248 Ser101. Energies were computed at the B3LYP/BS2 level and do not include zero-point
249 vibrational effects.

	Butyl quinoline[a]	Methyl quinoline[a]	Methyl quinoline[b]
C_3-C_2 distance (Å)	1.71	1.77	1.749
O-O distance (Å)	1.99	2.09	2.055
TS energy vs. $^1I_2$ (kcal·mol^{-1}) in water	8.1	11.3	8.0
TS energy vs. $^1I_2$ (kcal·mol^{-1}) (ε=5.7)	8.0	11.4	8.4

Ser101 – O_4 distance (Å)	1.57	1.58	1.741
His251 – O distance (Å)	1.89	1.83	Not applicable

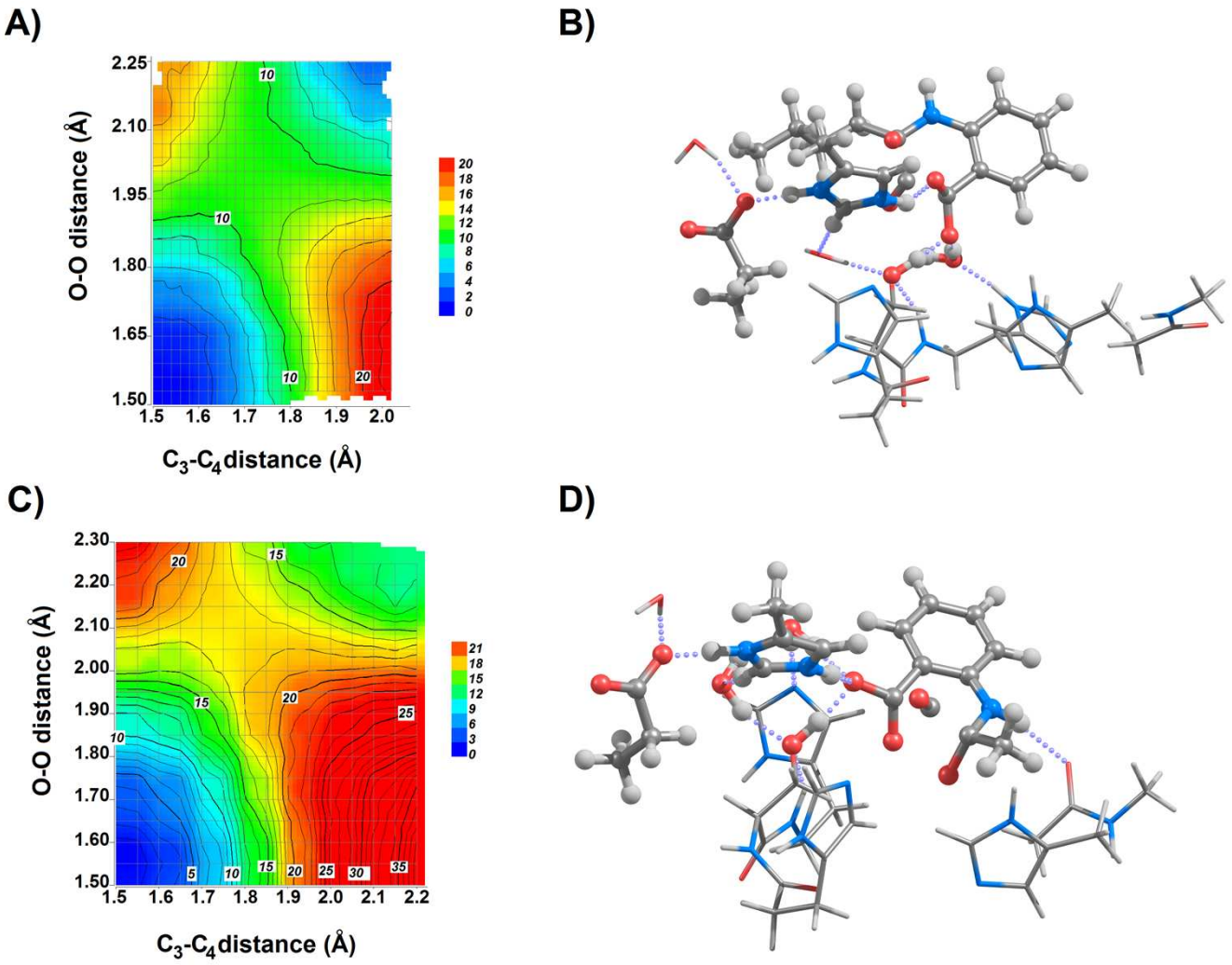

Figure 4: Newly-derived potential energy surfaces (at the B3LYP/6-31G(d) theory level) of the $^1I_2$→product reaction step for the A) butyl-, and C) methyl-substituted 4-oxoquinolines. Geometries of the transition states for the $^1I_2$→product reaction step for the B) butyl-, and D)

methyl-substituted 4-oxoquinolines are shown, with the substrate and sidechains of Ser101, Asp126 and His251 highlighted. Trp160 has been omitted from the images for clarity.

Other oxygenases

The experimental observation of EPR radical signals in anaerobic urate oxidase preparations upon incubation with uric acid (Gabison et al., 2011) is thought to support a reaction mechanism where urate dianion (generated through deprotonation of uric acid at the enzyme active site) transfers an electron to aminoacid sidechains (Lys, Arg or His) and reaction with O_2 occurs through electron transfer from these aminoacid radicals. Our DFT computations (Table 5) show that direct electron from the urate dianion to O_2 has such a low activation energy that no electron transfer to an active site aminoacid needs to occur to enable catalysis, and no minimum-energy crossing point between the singlet and triplet surfaces needs to be reached. The radical observed anaerobically (which may be His-based) should therefore play no role in the catalytic mechanism.

Finally, we computed the activation energy for the electron transfer between vitamin K and O_2. The value obtained (5.3 kcal·mol^{-1} in chlorobenzene, 3.3 kcal·mol^{-1} in water) is, again, inferior to the energy of the minimum-energy crossing point between the singlet and triplet surfaces (15.3 kcal·mol^{-1} in water (Silva & Ramos, 2007)). It thus appears that for all cofactor-less oxidases studied computationally so far (urate oxidase, ring-cleaving 2,4-dioxygenase, coproporphyrinogen oxidase and vitamin K-dependent glutamate carboxylase) catalysis occurs through direct electron transfer from substrate to O_2 followed by radical recombination, instead of minimum-energy crossing points without formal electron transfer.

Table 5: Reaction energies and activation energies of the electron-transfer from urate dianion to dioxygen or aminoacid sidechains, at the B3LYP/BS2//B3LYP/BS1 level.

	In chlorobenzene		In water	
Electron acceptor	Activation Energy (kcal·mol^{-1})	Reaction Energy (kcal·mol^{-1})	Activation Energy (kcal·mol^{-1})	Reaction energy (kcal·mol^{-1})
O_2	0.8	-9.3	4.2	0.1
His^+	18.8	17.0	48.1	47.5
Lys^+	34.3	30.9	65.2	64.3
Arg^+	24.5	20.5	51.5	51.4

Conclusions

The computations described in this paper show that the previously postulated triplet endoperoxide intermediate ($^3I_1$) is most unlikely to play a role in the reaction mechanism of bacterial ring-cleaving 2,4-dioxygenase, as the minimum energy crossing point between the singlet and triplet surfaces directly connects the reactants to the singlet endoperoxide intermediate ($^1I_1$). Moreover, the computed activation energy for the direct electron transfer from substrate to O_2 is lower than the MECP energy for substrates bearing electron-donating or weak electron-withdrawing groups at the 2- position, enabling flavin-like reactivity only after the 3-hydroxy group in the substrate is suitably deprotonated by the His251/Asp126 dyad (Table2).

Reactivity with substrates bearing long alkyl chains on the 2-position is not possible in the originally postulated position: it instead relies on a different binding mode which enables catalysis of the CO release step by positioning the nascent negative charges in a suitably stabilizing environment.

References

Becke AD. 1993. Density-functional thermochemistry. III. The role of exact exchange. *The Journal of Chemical Physics* 98:5648–5652.

Bui S., von Stetten D., Jambrina PG., Prangé T., Colloc'h N., de Sanctis D., Royant A., Rosta E., Steiner RA. 2014. Direct evidence for a peroxide intermediate and a reactive enzyme-substrate-dioxygen configuration in a cofactor-free oxidase. *Angewandte Chemie (International ed. in English)* 53:13710–4.

Cossi M., Mennucci B., Pitarch J., Tomasi J. 1998. Correction of cavity-induced errors in polarization charges of continuum solvation models. *Journal of Computational Chemistry* 19:833–846.

Ferguson-Miller S., Babcock GT. 1996. Heme/Copper Terminal Oxidases. *Chemical Reviews* 96:2889–2908.

Fetzner S., Steiner RA. 2010. Cofactor-independent oxidases and oxygenases. *Applied microbiology and biotechnology* 86:791–804.

Gabison L., Chopard C., Colloc'h N., Peyrot F., Castro B., Hajji M El., Altarsha M., Monard G., Chiadmi M., Prangé T. 2011. X-ray, ESR, and quantum mechanics studies unravel a spin well in the cofactor-less urate oxidase. *Proteins: Structure, Function, and Bioinformatics* 79:1964–1976.

Granovsky AA. 2013. Firefly 8.0.0.

Hansch C., Leo a., Taft RW. 1991. A Survey of Hammett Substituent Constants and Resonance and Field Parameters. *Chemical Reviews* 91:165–195.

Harvey JN. 2007. Understanding the kinetics of spin-forbidden chemical reactions. *Physical chemistry chemical physics : PCCP* 9:331–43.

Harvey JN. 2014. Spin-forbidden reactions: Computational insight into mechanisms and kinetics. *Wiley Interdisciplinary Reviews: Computational Molecular Science* 4:1–14.

Harvey JN., Aschi M., Schwarz H., Koch W. 1998. The singlet and triplet states of phenyl cation. A hybrid approach for locating minimum energy crossing points between non-interacting potential energy surfaces. *Theoretical Chemistry Accounts: Theory, Computation, and Modeling (Theoretica Chimica Acta)* 99:95–99.

Hernandez-Ortega A., Quesne MG., Bui S., Heuts DPHM., Steiner RA., Heyes DJ., De Visser SP., Scrutton NS. 2014. Origin of the proton-transfer step in the cofactor-free (1H)-3-hydroxy-4-oxoquinaldine 2,4-dioxygenase: Effect of the basicity of an active site his residue. *Journal of Biological Chemistry* 289:8620–8632.

Hernández-Ortega A., Quesne MG., Bui S., Heyes DJ., Steiner R a., Scrutton NS., de Visser SP. 2015. Catalytic Mechanism of Cofactor-Free Dioxygenases and How They Circumvent Spin-Forbidden Oxygenation of Their Substrates. *Journal of the American Chemical Society* 137:7474–7487.

Hertwig RH., Koch W. 1995. On the accuracy of density functionals and their basis set dependence: An extensive study on the main group homonuclear diatomic molecules Li2 to Br2. *Journal of Computational Chemistry* 16:576–585.

Krieger E., Vriend G. 2014. YASARA View--molecular graphics for all devices--from smartphones to workstations. *Bioinformatics* 30:2981–2982.

Lee C., Yang W., Parr RG. 1988. Development of the Colle-Salvetti correlation-energy formula into a functional of the electron density. *Physical Review B* 37:785–789.

Löwdin P-O. 1970. On the nonorthogonality problem. In: *Advances in Quantum Chemistry, Vol. 5*. 185–199.

Marian C. 2001. Spin-orbit coupling in molecules. *Reviews in computational chemistry* 17:99–204.

Massey V. 1994. Activation of molecular oxygen by flavins and flavoproteins. *The Journal of biological chemistry* 269:22459–62.

Mennucci B., Tomasi J. 1997. Continuum solvation models: A new approach to the problem of solute's charge distribution and cavity boundaries. *Journal of Chemical Physics* 106:5151–5158.

Mulliken RS. 1955. Electronic Population Analysis on LCAO-MO Molecular Wave Functions. I. *The Journal of Chemical Physics* 23:1833.

Nakamura H. 1987. Semiclassical treatment of nonadiabatic transitions: Multilevel curve crossing and nonadiabatic tunneling problems. *The Journal of Chemical Physics* 87:4031.

Prabhakar R., Siegbahn PEM., Minaev BF., Ågren H. 2002. Activation of Triplet Dioxygen by Glucose Oxidase: Spin−Orbit Coupling in the Superoxide Ion. *The Journal of Physical Chemistry B* 106:3742–3750.

Que L., Ho RYN. 1996. Dioxygen Activation by Enzymes with Mononuclear Non-Heme Iron Active Sites. *Chemical Reviews* 96:2607–2624.

Schmidt MW., Baldridge KK., Boatz JA., Elbert ST., Gordon MS., Jensen JH., Koseki S., Matsunaga N., Nguyen KA., Su S. et al. 1993. General atomic and molecular electronic structure system. *Journal of Computational Chemistry* 14:1347–1363.

Silva PJ. 2014. With or without light: comparing the reaction mechanism of dark-operative protochlorophyllide oxidoreductase with the energetic requirements of the light-dependent protochlorophyllide oxidoreductase. *PeerJ* 2:e551.

Silva PJ., Ramos MJ. 2007. Reaction Mechanism of the Vitamin K-Dependent Glutamate Carboxylase: A Computational Study. *The Journal of Physical Chemistry B* 111:12883–

12887.

Silva PJ., Ramos MJ. 2008. A comparative density-functional study of the reaction mechanism of the O2-dependent coproporphyrinogen III oxidase. *Bioorganic & medicinal chemistry* 16:2726–33.

Silva PJ., Ramos MJ. 2009. Computational studies on the reactivity of substituted 1,2-dihydro-1,2-azaborines. *The Journal of Organic Chemistry* 74:6120–6129.

Sono M., Roach MP., Coulter ED., Dawson JH. 1996. Heme-Containing Oxygenases. *Chemical Reviews* 96:2841–2888.

Steiner RA., Janssen HJ., Roversi P., Oakley AJ., Fetzner S. 2010. Structural basis for cofactor-independent dioxygenation of N-heteroaromatic compounds at the alpha/beta-hydrolase fold. *Proceedings of the National Academy of Sciences of the United States of America* 107:657–62.

Thierbach S., Bui N., Zapp J., Chhabra SR., Kappl R., Fetzner S. 2014. Substrate-assisted O2 activation in a cofactor-independent dioxygenase. *Chemistry & biology* 21:217–25.

Tomasi J., Persico M. 1994. Molecular Interactions in Solution: An Overview of Methods Based on Continuous Distributions of the Solvent. *Chemical Reviews* 94:2027–2094.

Trott O., Olson AJ. 2010. AutoDock Vina: improving the speed and accuracy of docking with a new scoring function, efficient optimization, and multithreading. *Journal of computational chemistry* 31:455–61.

Wallar BJ., Lipscomb JD. 1996. Dioxygen Activation by Enzymes Containing Binuclear Non-Heme Iron Clusters. *Chemical Reviews* 96:2625–2658.

Wijaya IMM., Domratcheva T., Iwata T., Getzoff ED., Kandori H. 2016. Single Hydrogen Bond Donation from Flavin N 5 to Proximal Asparagine Ensures FAD Reduction in DNA Photolyase. *Journal of the American Chemical Society* 138:4368–4376.

Yachandra VK., Sauer K., Klein MP. 1996. Manganese Cluster in Photosynthesis: Where Plants Oxidize Water to Dioxygen. *Chemical Reviews* 96:2927–2950.